

pubs.acs.org/JPCL Letter

# Role of Solid-State Miscibility during Anion Exchange in Cesium Lead Halide Nanocrystals Probed by Single-Particle Fluorescence

Dong Wang, John Cavin, Bo Yin, Arashdeep S. Thind, Albina Y. Borisevich, Rohan Mishra, and Bryce Sadtler\*



Cite This: J. Phys. Chem. Lett. 2020, 11, 952–959



**ACCESS** 

III Metrics & More

Article Recommendations

Cs Pb Cl Br

N(C<sub>4</sub>H<sub>9</sub>)<sub>4</sub>Br

N(C<sub>4</sub>H<sub>9</sub>)<sub>4</sub>Cl

Single-particle intensity

Supporting Information

ABSTRACT: In this Letter, we used fluorescence microscopy to image the reversible transformation of individual CsPbCl<sub>3</sub> nanocrystals to CsPbBr<sub>3</sub>, which enables us to quantify heterogeneity in reactivity among hundreds of nanocrystals prepared within the same batch. We observed a wide distribution of waiting times for individual nanocrystals to react as has been seen previously for cation exchange and ion intercalation. However, a significant difference for this reaction is that the switching times for changes in fluorescence intensity are dependent on the concentration of substitutional halide ions in solution (i.e., Br<sup>-</sup> or Cl<sup>-</sup>). On the basis of the high solid-state miscibility between CsPbCl<sub>3</sub> and CsPbBr<sub>3</sub>, we develop a model in which the activation energy for anion exchange depends on the density of exchanged ions in the nanocrystal. The heterogeneity in reaction kinetics observed among individual nanocrystals limits the compositional uniformity that can be achieved in luminescent CsPbCl<sub>3-x</sub>Br<sub>x</sub> nanocrystals prepared by anion exchange.

olloidal cesium lead halide nanocrystals (CsPbX<sub>3</sub>, where X = Cl, Br, or I) display high photoluminescence (PL) quantum yields without the need for postsynthetic processing. 1-9 The wavelength of emission can be tuned across the visible range on the basis of their size and composition, making these materials of significant interest for applications in light emission, such as light-emitting diodes and lasers. 10-12 Anion exchange provides a facile method for tuning the halide composition and band gap of CsPbX<sub>3</sub> and CH<sub>3</sub>NH<sub>3</sub>PbX<sub>3</sub> nanocrystals (NCs).<sup>6,7,13-16</sup> Similar to other solid-state transformations in nanocrystals (e.g., cation exchange and ion intercalation), 17-28 the high surface-to-volume ratio and diffusion coefficients of ions enable this reaction to take place both rapidly (i.e., on the time scale of seconds to minutes) and reversibly. For applications in solid-state lighting, it is desirable to synthesize lead halide perovskite nanocrystals of uniform size and composition as heterogeneity in these parameters decreases the color purity. However, the interconversion between CsPbX<sub>3</sub> nanocrystals of different halide compositions via anion exchange exhibits complex reaction kinetics. Both the lattice constants and the PL emission wavelength have been observed to go through different rates of change as the reaction progresses. 29,30 These changes in reaction rate are supported by first-principles calculations that indicate CsPbCl<sub>3-x</sub>Br<sub>x</sub> and CsPbBr<sub>3-x</sub>I<sub>x</sub> mixed-halide crystals with x = 2 are more stable than other halide compositions and may act as an intermediate phase to hinder a continuous transformation. 30-32 Furthermore, the kinetics for the CsPbBr<sub>3</sub>/CsPbI<sub>3</sub> exchange pair have been shown to be sensitive to the surface chemistry of the nanocrystals and the method used to monitor the reaction (e.g., diffraction or

photoluminescence). These observations suggest that fundamental studies of the kinetics of anion exchange in individual CsPbX<sub>3</sub> nanocrystals are needed to facilitate their production and incorporation into optoelectronic devices.

While anion exchange exhibits similarities to other chemical transformations in colloidal semiconductor nanocrystals, a unique feature of this reaction is the complete solid-state miscibility exhibited between CsPbCl<sub>3</sub> and CsPbBr<sub>3</sub>. 31,32 In this study, we aimed to determine how this high miscibility affects the reaction trajectories of individual nanocrystals undergoing anion exchange. Single-nanocrystal fluorescence microscopy has been used to understand how heterogeneity among a population of particles leads to the observed ensemble behavior. \$\frac{8}{9},21-23,33-45\$ Thus, we used changes in the emission wavelength and intensity as a signature for when individual NCs undergo this transformation. We observed distinct differences for this system compared to related solid-state transformations in which the initial and final crystals lack solid solubility. 21-23 On the basis of our observations and previous ensemble kinetic studies, we develop a model in which the decrease in the activation barrier for successive anion exchange events is more gradual than systems that require a phase transformation. Our results imply that the stochastic nature of

Received: December 8, 2019 Accepted: January 16, 2020 Published: January 16, 2020



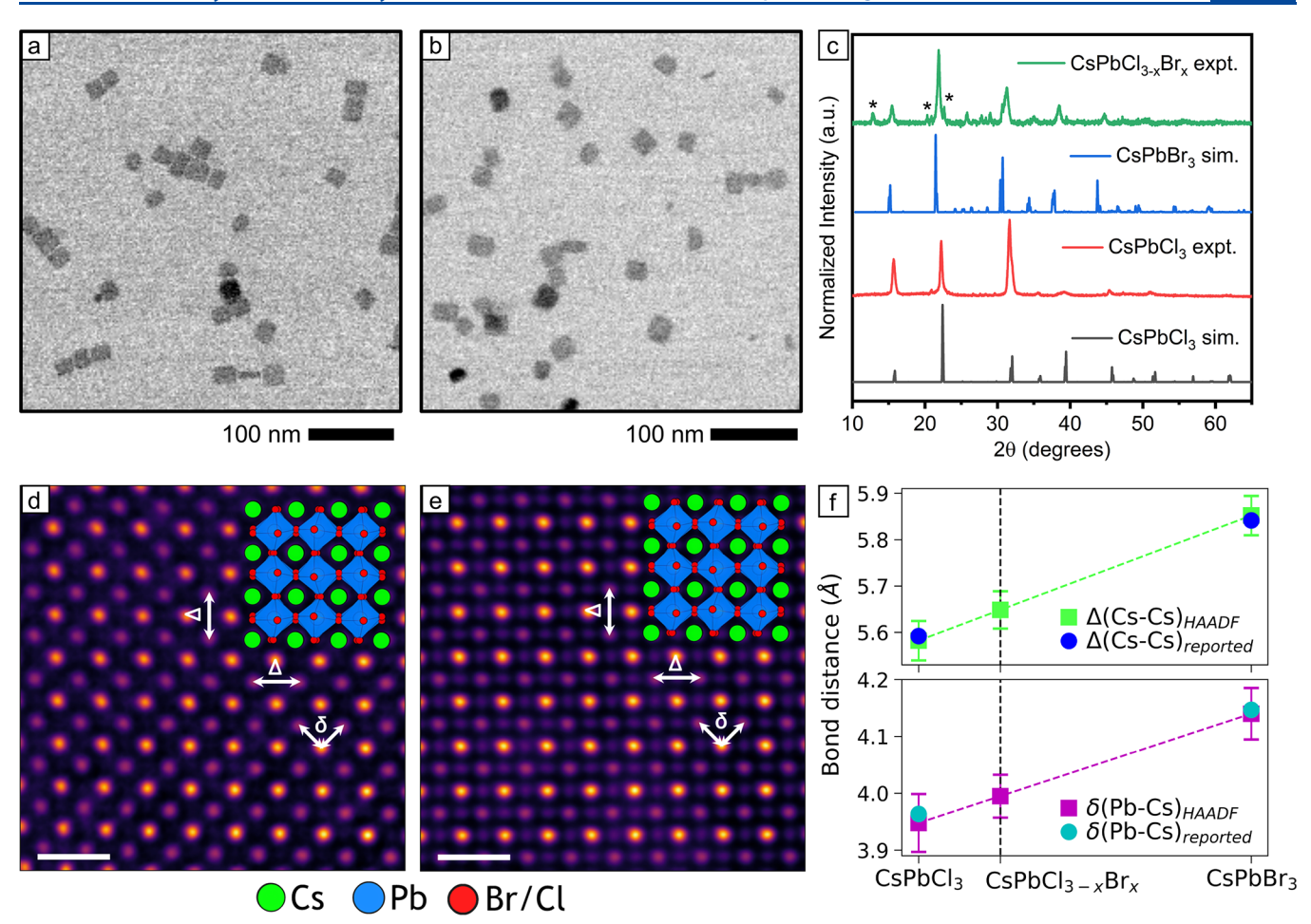


Figure 1. (a) Bright field TEM image of the as-synthesized CsPbCl $_3$  nanocrystals. (b) Bright field TEM image of CsPbCl $_{3-x}$ Br $_x$  nanocrystals after anion exchange. (c) XRD patterns of the as-synthesized CsPbCl $_3$  nanocrystals (red) and the CsPbCl $_{3-x}$ Br $_x$  nanocrystals (green) after anion exchange. The blue and gray traces show simulated powder XRD patterns made using ICSD collection codes 243735 for CsPbBr $_3$  and 243734 for CsPbCl $_3$ . The peaks marked with asterisks correspond to Cs $_4$ PbBr $_6$ . Atomic-resolution STEM-HAADF images of (d) a CsPbCl $_3$  nanocrystal and (e) a CsPbCl $_{3-x}$ Br $_x$  nanocrystal with their overlaid atomic model showing the [101] projection of the crystal structure. Scale bars correspond to 1 nm. (f) Comparison of the change in bond distances for different anion compositions as obtained from STEM-HAADF and those provided in a previous report. Firor bars correspond to one standard deviation in the spacing measurements.

reactivity among individual nanocrystals limits the compositional uniformity that is possible in CsPbCl<sub>3-x</sub>Br<sub>x</sub> nanocrystals prepared by anion exchange.

Figure 1a shows a bright field transmission electron microscopy (TEM) image of  $CsPbCl_3$  NCs synthesized using the method of Kovalenko and co-workers. The NCs are platelet-shaped with an average edge length of  $19.1 \pm 5.0$  nm (average  $\pm$  first standard deviation). The  $CsPbCl_3$  NCs were converted to cesium lead chlorobromide ( $CsPbCl_{3-x}Br_x$ ) NCs on a TEM grid via anion exchange using tetrabutylammonium bromide (TBAB) as the source of bromide anions. As shown in Figure 1b, the shape and size of the  $CsPbCl_{3-x}Br_x$  NCs, which have an average edge length of  $19.4 \pm 3.9$  nm (average  $\pm$  first standard deviation), were preserved after anion exchange. The Supporting Information provides detailed experimental procedures for synthesizing  $CsPbCl_3$  NCs and converting them to  $CsPbBr_3$  as well as histograms showing the edge lengths before and after anion exchange (Figure S1).

Figure 1c shows powder X-ray diffraction (XRD) patterns of the CsPbCl<sub>3</sub> NCs before and after anion exchange. The XRD pattern of the CsPbCl<sub>3</sub> NCs matched the expected diffraction pattern for orthorhombic CsPbCl<sub>3</sub>. Peaks in the XRD pattern of the converted CsPbCl<sub>3-x</sub>Br<sub>x</sub> NCs showed a shift to smaller

angles compared to the pattern for CsPbCl<sub>3</sub>. However, the peaks for the product NCs were still at larger angles relative to the expected diffraction pattern for orthorhombic CsPbBr3, which indicates that the product NCs contain residual chloride ions. The presence of chloride in the product NCs following anion exchange was further confirmed by X-ray photoelectron spectroscopy (XPS) (see Figure S3 and Table S2). Assuming a linear shift in the lattice constants with anion composition, as reported for alloys using first-principles calculations,<sup>31</sup> the approximate composition after anion exchange is CsPbClBr<sub>2</sub> (i.e., x = 2). The presence of  $Cs_4PbBr_6$  as an impurity was observed when the CsPbCl<sub>3-x</sub>Br<sub>x</sub> NCs were prepared for XRD analysis in which a higher concentration of NCs was used than for TEM and fluorescence microscopy (Figure 1c and Figure S2). 24-27 As Cs<sub>4</sub>PbBr<sub>6</sub> has been reported to be nonfluorescent at visible wavelengths, <sup>24–27</sup> this impurity phase does not show up in the fluorescence microscopy studies described below.

To further investigate the localized structural changes occurring within individual nanocrystals as a result of the anion exchange, we have performed atomic-resolution scanning transmission electron microscopy (STEM) imaging. Panels d and e of Figure 1 show atomic-resolution high-angle annular dark field (HAADF) images of single CsPbCl<sub>3</sub> and

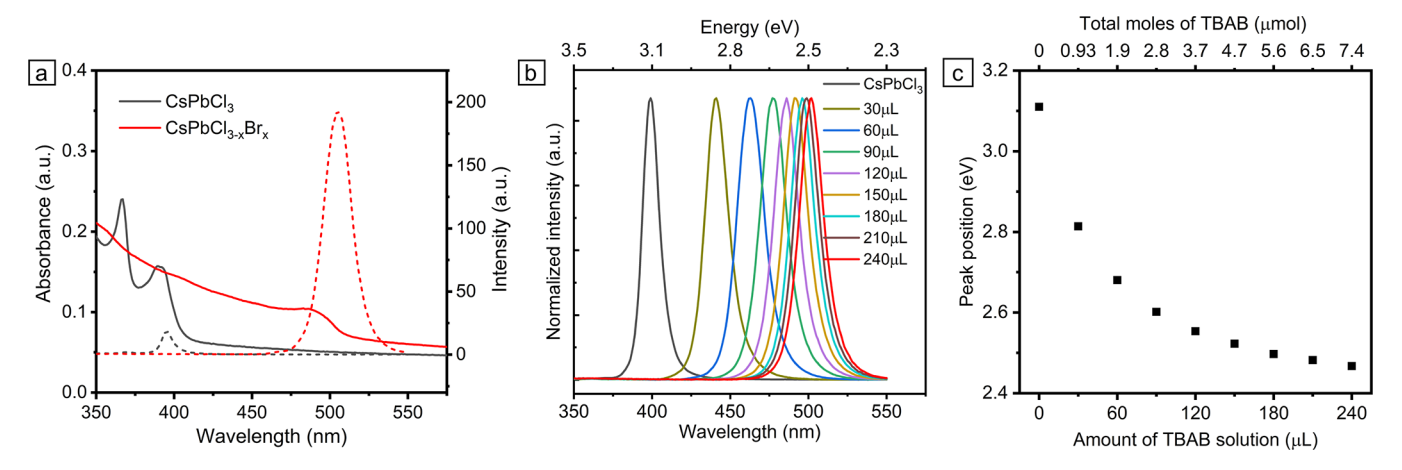


Figure 2. (a) UV-vis absorption (solid lines) and PL (dashed lines) spectra of CsPbCl<sub>3</sub> nanocrystals dispersed in hexane before and after anion exchange. The spectra of the initial CsPbCl<sub>3</sub> nanocrystals are colored gray, and the spectra of the CsPbCl<sub>3-x</sub>Br<sub>x</sub> nanocrystals are colored red. (b) Normalized PL spectra of CsPbCl<sub>3</sub> nanocrystals after the addition of increasing amounts of a TBAB solution in tert-butanol with a concentration of 10 mg/mL (31 mmol/L). Sixty microliters of the stock solution of CsPbCl<sub>3</sub> NCs was diluted by a factor of 50 for the ensemble anion exchange experiments. (c) Energies of the PL maxima for the same CsPbCl<sub>3-x</sub>Br<sub>x</sub> nanocrystals as a function of the amount of TBAB added. The excitation wavelength was 300 nm for all PL spectra. Values of the peak positions and their corresponding full widths at half-maximum are provided in Table S1.

CsPbCl<sub>3-x</sub>Br<sub>x</sub> nanocrystals, respectively, viewed along the [101] direction of the orthorhombic polymorph. In this imaging mode, the intensity of individual atomic columns is approximately proportional to the squared atomic number ( $\sim Z^2$ ) of the column. 46 Hence, the brightest atomic columns correspond to Pb-(Cl/Br) followed by the Cs atomic columns. The lighter Cl (Z = 17) atomic columns in CsPbCl<sub>3</sub> (Figure 1d) are not visible as they cause weak elastic scattering of the electrons. However, the mixed Cl/Br columns in CsPbCl<sub>3-x</sub>Br<sub>x</sub> (Figure 1e) are visible because of the heavier Br atoms (Z = 35). We do not observe any discernible segregation of Cl/Br ions, which would have resulted in missing anion columns that were rich in Cl. As shown in Figure 1c, the anion exchange process is accompanied by the shifts in the XRD pattern to smaller angles because of the increase in the lattice constant of the ensemble as the concentration of Br increases. On the basis of STEM-HAADF image analysis, we provide the changes in Cs–Cs ( $\Delta$ ) and Pb– Cs  $(\delta)$  in-plane bond distances within individual CsPbCl<sub>3</sub>, CsPbCl<sub>3-x</sub>Br<sub>x</sub>, and CsPbBr<sub>3</sub> nanocrystals in Figure 1f and compare them with previously reported bond distances.<sup>47</sup> The average  $\Delta$  values (Cs-Cs) from HAADF images for CsPbCl<sub>3</sub> and CsPbBr<sub>3</sub> nanocrystals are  $5.58 \pm 0.04$  and  $5.85 \pm 0.04$  Å, respectively, which compares well with the reported values of 5.59 and 5.84 Å, respectively. Similarly,  $\delta$  values (Pb-Cs) from HAADF images for CsPbCl<sub>3</sub> and CsPbBr<sub>3</sub> nanocrystals are 3.95  $\pm$  0.05 and 4.14  $\pm$  0.05 Å, respectively. They are in good agreement with the reported values of 3.96 and 4.14 Å for CsPbCl<sub>3</sub> and CsPbBr<sub>3</sub>, respectively. Both  $\Delta$  (Cs-Cs) and  $\delta$ (Pb-Cs) increase as the concentration of Br increases, and the values of  $\Delta$  (5.65  $\pm$  0.04 Å) and  $\delta$  (4.00  $\pm$  0.04 Å) for CsPbCl<sub>3-x</sub>Br<sub>x</sub> are intermediate between the two end members. Using Vegard's law, both measurements lead to an average composition with  $x = 0.76 \pm 0.04$ . Thus, STEM-HAADF imaging reveals a steady lattice expansion of individual NCs upon Cl/Br exchange with no apparent clustering of the halide ions.

Optical spectroscopy was next used to monitor anion exchange in CsPbX3 NCs based on systematic shifts in the optical band gap with composition. 1,4,6,13 Figure 2a shows ultraviolet-visible (UV-vis) absorption and PL spectra of colloidal solutions of both CsPbCl<sub>3</sub> and CsPbCl<sub>3-x</sub>Br<sub>x</sub> NCs. The

maxima in the first exciton absorption peak shifted from 390 nm for the initial CsPbCl<sub>3</sub> NCs to 492 nm after anion exchange, similar to previous reports. 1,2,6,13 Furthermore, the integrated PL intensity increased by >30 times after anion exchange, consistent with the higher PL quantum yield typically exhibited by CsPbBr<sub>3</sub> compared to CsPbCl<sub>3</sub> NCs. Both the initial NCs and the product NCs exhibit weak quantum confinement based on the appearance of exciton peaks and the blue shift of the fluorescence maxima relative to the bulk band gaps of CsPbCl<sub>3</sub> and CsPbBr<sub>3</sub>. Although the average edge length of the platelet nanocrystals is >19 nm, the thicknesses of the nanoplates vary from 3 to 5 nm (see Figure S4), which leads to quantum confinement, similar to previous reports. <sup>3,6,36,48</sup> Figure 2b shows the change in PL spectra after successive aliquots of TBAB were added to a colloidal solution of CsPbCl<sub>3</sub> nanocrystals. The maxima in the PL spectra red-shifted continuously from 398 nm (3.12 eV) to 505 nm (2.46 eV) as the total amount of TBAB added was increased (Figure 2c). The full widths at halfmaximum for the PL spectra varied between 0.09 and 0.13 eV (see Table S1). This gradual shifting is a result of the high miscibility of CsPbCl<sub>3</sub> and CsPbBr<sub>3</sub> along with rapid exchange kinetics for nanoscale crystals such that the anion composition in the nanocrystal lattice reflects the overall ratio of Cl- to Branions. 13,15,29

We used the red shift and increase in PL intensity upon anion exchange from Cl<sup>-</sup> to Br<sup>-</sup> to monitor this transformation in single NCs by fluorescence microscopy. The experimental setup is similar to that used in our previous studies on ion intercalation in PbBr<sub>2</sub> nanocrystals<sup>23</sup> as well as work by Routzahn and Jain on cation exchange in CdSe nanocrystals. 21,22 The Supporting Information provides further details of the procedure and a schematic of the experimental setup (Figure S6). Briefly, the stock solution of CsPbCl<sub>3</sub> NCs is diluted (250-fold) and spincoated onto a microscope coverslip that forms the bottom half of a flow cell. A TBAB solution of varying concentration (from 1 to 10 μg/mL) dissolved in 1-octadecene (ODE) and tert-butanol (25:1 volume ratio) is then introduced into the flow cell using a syringe pump. Ultraviolet illumination (315–380 nm) is sent through the objective of an inverted microscope to photoexcite NCs on the coverslip. However, an emission filter cuts off emission from the CsPbCl<sub>3</sub> NCs, so the initial field of view is

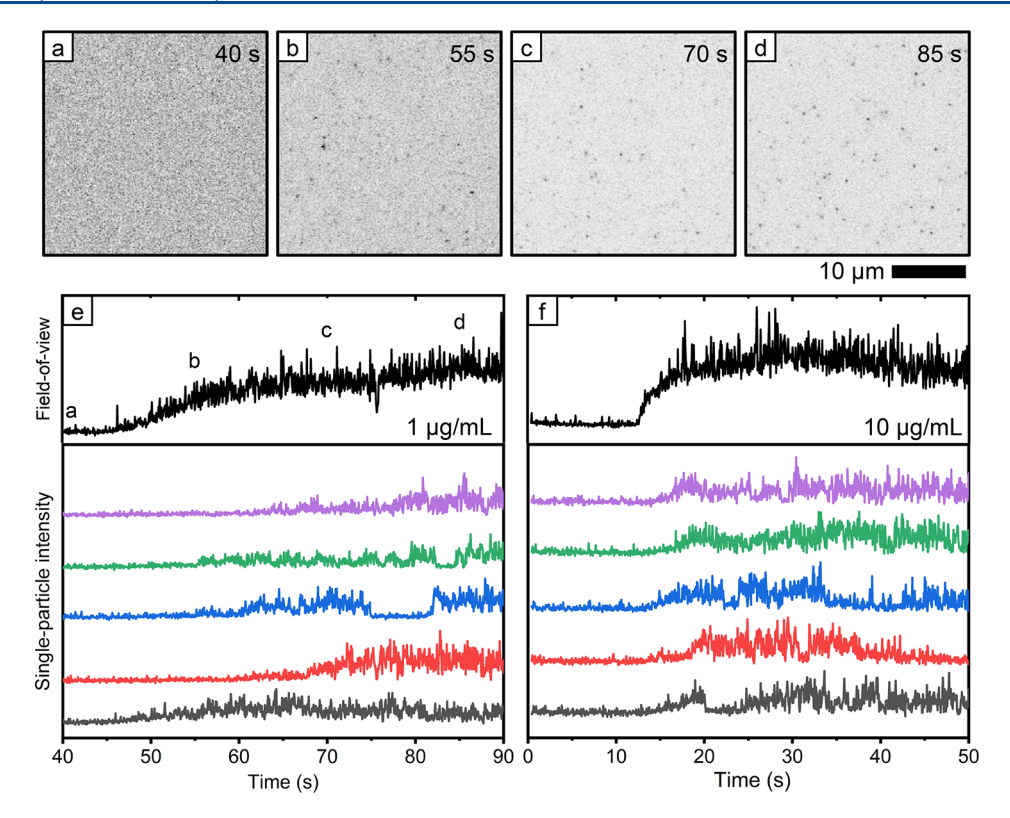


Figure 3. (a–d) Selected frames from a fluorescence video recording during the transformation of CsPbCl<sub>3</sub> nanocrystals to CsPbCl<sub>3-x</sub>Br<sub>x</sub> at a TBAB concentration of 1  $\mu$ g/mL (3.1  $\mu$ mol/L). The scale bar of 10  $\mu$ m applies to all four images; the contrast of the images has been inverted, and only a portion of the entire microscope field of view is shown. (e) Integrated intensity vs time over the entire field of view (top) using a TBAB concentration of 1  $\mu$ g/mL along with representative trajectories for individual nanocrystals (bottom). (f) Integrated intensity and single-particle intensities using a TBAB concentration of 10  $\mu$ g/mL (31.1  $\mu$ mol/L). The time points shown in the top right corner of panels a–d as well as the x-axes of panels e and f were measured relative to when the TBAB solution was injected into the flow cell.

dark. While there is heterogeneity in the fluorescence maximum for different nanocrystals, our ability to watch individual nanocrystals undergo anion exchange relies on the large spectral shift ( $\sim 100 \text{ nm}$ ) and increased fluorescence brightness during this reaction. After the TBAB solution is introduced, fluorescent spots begin to appear in the field of view, indicating the transformation of CsPbCl<sub>3</sub> NCs to CsPbCl<sub>3-x</sub>Br<sub>x</sub> NCs (see the Supporting Movie).

Figure 3a—d shows a section of the microscope field of view at different times during the transformation of individual NCs at a TBAB concentration of 1  $\mu$ g/mL (3.1  $\mu$ mol/L); a typical field of view contained ~500 NCs. Changes in fluorescence intensity integrated over of the entire field of view following the introduction of TBAB are shown in panels e and f of Figure 3 for two different TBAB concentrations (1 and 10  $\mu$ g/mL). The integrated intensity rise is more abrupt at the higher TBAB concentration. For TBAB concentrations of <1  $\mu$ g/mL, the appearance of bright fluorescent spots was not observed. At TBAB concentrations of >10  $\mu$ g/mL (31  $\mu$ mol/L), emission from individual NCs was observed to degrade at a time scale similar to that of the transformation. We used a light intensity (15  $\mu$ W/cm<sup>2</sup> at 350 nm) that is lower than the intensities (milliwatts per square centimeter to watts per square centimeter) typically needed to observe photoinduced reactions in lead halide perovskite films, such as halide segregation. 9,49-52 Furthermore, we observed the same trends in single-particle reaction trajectories when using different excitation wavelengths and intensities (see the Supporting Discussion and Figure S15).

Representative intensity trajectories for individual NCs at different TBAB concentrations are shown in panels e and f of Figure 3. Once the exchange reaction has occurred, emission from individual CsPbCl<sub>3-x</sub>Br<sub>x</sub> NCs exhibited fluorescence intermittency as has been previously observed for lead halide perovskite nanocrystals. <sup>38–42</sup> Blinking in CsPbCl<sub>3–x</sub>Br<sub>x</sub> NCs prepared by in situ anion exchange under the microscope was similar to that of NCs that were converted prior to imaging (Figure S8). TEM images at different dilution factors (see Figure S7) indicate that the particle concentration used for fluorescence microscopy led to well-dispersed nanocrystals with few clusters. Furthermore, clusters of nanocrystals with overlapping emission profiles within a diffraction-limited region could be distinguished from single nanocrystals based on their intensity profiles (Figures S9 and S10)44,45 and were removed from subsequent analysis. A wide range of turn-on times was observed for different NCs within the same field of view, similar to other solid-state transformations that have been studied by fluorescence microscopy.  $^{21-23}$  At the flow rate used in these experiments (7.5 mL/h), the turn-on times for individual NCs were not correlated with their location (Figure S11). Thus, the slow rise in the integrated intensity for the ensemble of NCs is attributed to the stochastic nature of turn-on events for individual NCs.

To quantify differences in the fluorescence trajectories of individual NCs, the time needed for each NC to reach a threshold intensity (three standard deviations above the noise) was measured for hundreds of NCs at different concentrations of TBAB. We refer to this value as the waiting time for the NC to

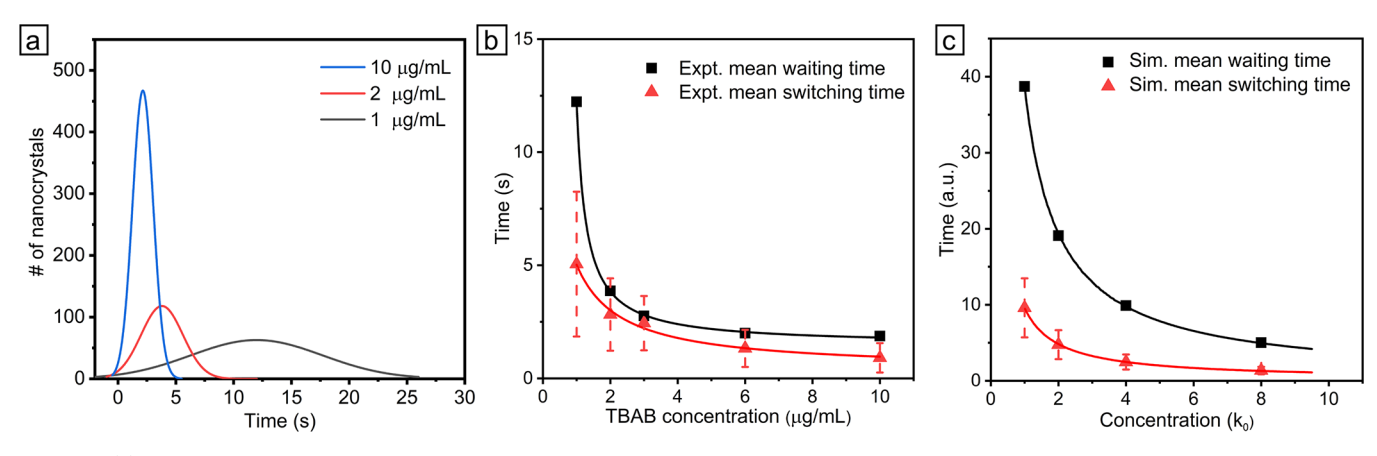


**Figure 4.** (a) Gaussian fits to distributions of relative waiting times for single NCs following anion exchange using different concentrations of TBAB. The original histograms are shown in Figure S12. (b) Experimental mean relative waiting times (black squares) and switching times (red triangles) for anion exchange in single NCs as a function of TBAB concentration. The error bars represent one standard deviation in the distribution of switching times. The lines show fits to the concentration dependencies of the form y = [a/(x+b)] + c, where  $a = 3 \text{ s } \mu \text{g/mL}^{-1}$ ,  $b = -0.7 \mu \text{g/mL}$ , and c = 1.5 s for the waiting times and  $a = 6 \text{ s } \mu \text{g/mL}^{-1}$ ,  $b = 0.3 \mu \text{g/mL}$ , and c = 0.4 s for the switching times. (c) Simulated median waiting times (black squares) and switching times (red triangles) using the exchange-density model as a function of concentration. The solid lines show fits to the concentration dependencies of the form a/x + c, where a = 40 and c = 0.15 for the waiting times and a = 9.8 and c = 0.12 for the switching times in arbitrary units.

turn on. To compare the distribution of waiting times at different concentrations of TBAB, the first NC to turn on at a given TBAB concentration was assigned a waiting time of 0, and the waiting times for all other NCs in the field of view were measured relative to the first one. Histograms of the relative waiting times for single NCs transformed using different concentrations of TBAB are plotted in Figure S12. These distributions were fit to Gaussian functions as shown in Figure 4a. The distributions of waiting times show a strong dependence on the TBAB concentration. As the TBAB concentration increases, both the mean relative waiting time and the full width at half-maximum (fwhm) of the Gaussian fit decrease (Figure S13).

The waiting time for each NC to turn on includes an "incubation time" in which the TBAB solution has entered the field of view, but the NC has not yet started to transform. To exclude the incubation component, we next fit the intensity rise for each NC trajectory to a sigmoidal function to extract the switching time,  $\tau$ , for the NC. <sup>21–23</sup> A sharper intensity rise will lead to a smaller switching time. As shown in Figure 4b, both the mean value of single-NC switching times and the standard deviation in the distribution of switching times decrease as the TBAB concentration increases. Thus, the sharper integrated intensity rise for the ensemble of NCs at higher TBAB concentrations (see Figure S14) results from both the narrowing of the distribution of waiting and switching times and their shift toward shorter times. While a systematic investigation of how the waiting and switching times depend on the shape and size of the NCs is ongoing, these same trends were observed for anion exchange in CsPbCl<sub>3</sub> NCs with larger average dimensions (Figure S16). We also investigated the back conversion of CsPbCl<sub>3-x</sub>Br<sub>x</sub> NCs to CsPbCl<sub>3</sub> with tetrabutylammonium chloride (TBAC) as the chloride source. Using the same analysis as described above for the forward transformation, the CsPbCl<sub>3-x</sub>Br<sub>x</sub> NCs are initially bright under the microscope and become dark after they transform into CsPbCl<sub>3</sub> (Figure S17 and Supporting Movie). Both the mean values of waiting times and switching times for the back exchange of single NCs show a similar dependence on the TBAB concentration as the forward transformation (Figure S18).

Single-particle fluorescence microscopy has been previously used to study cation exchange between CdSe and Ag<sub>2</sub>Se NCs as

well as the intercalation of CH3NH3Br into PbBr2 NCs to form CH<sub>3</sub>NH<sub>3</sub>PbBr<sub>3</sub>. <sup>21-23</sup> Waiting and switching times for these transformations were measured as a function of reactant concentration (i.e., AgNO<sub>3</sub> or CH<sub>3</sub>NH<sub>3</sub>Br). Similar to our results, in both cases, the distribution of waiting times narrowed as the reactant concentration increased. For all three reactions, the ensemble intensity rise comprises abrupt transitions for individual NCs that exhibit a distribution of incubation times before they transform. However, a significant difference observed in these prior cases was that the switching times were insensitive to the reactant concentration. We propose that differences in the solid-state miscibility between the initial and final crystals are responsible for the differences in switching times observed for these NC transformations. Both CdSe/Ag<sub>2</sub>Se and PbBr<sub>2</sub>/CH<sub>3</sub>NH<sub>3</sub>PbBr<sub>3</sub> crystal pairs lack solid solubility due to differences in the arrangement of ions before and after the reaction. 17,18 Thus, in both of these transformations, the new phase must first nucleate within the parent lattice. We previously simulated the effect of this phase transformation on waiting and switching times by incorporating an activation barrier for reaction events (e.g., ion intercalation or exchange) in a particle that decreased after a threshold number of events had been reached.<sup>23</sup> Monte Carlo trajectories were used to simulate the transformation of individual nanocrystals, and the probability for each reaction event depended on the free energy change for that step. When we incorporated a free energy change,  $\Delta G_i$  (where i is the number of reaction events in a trajectory), that decreased after a critical number of reaction events, the simulated waiting times decreased with reactant concentration while the switching times were insensitive to concentration, matching experimental observations for solid-state transformations that lack solid solubility.

In the case of anion exchange between CsPbCl<sub>3</sub> and CsPbBr<sub>3</sub>, the initial and final crystals possess complete solid miscibility due to their similarity in structure (both are orthorhombic) and anionic radii.  $^{13,32}$  Furthermore, activation barriers for halide diffusion in lead halide perovskites  $^{15,53}$  are smaller than for both  $\rm Cd^{2+}/Ag^{+}$  exchange in CdSe  $^{54}$  as well as for CH<sub>3</sub>NH<sub>3</sub> diffusion in lead halide crystals.  $^{15,53,55}$  The high diffusion coefficients of halide anions within CsPbX<sub>3</sub> crystals lead to a uniform composition within the nanocrystal as ions are exchanging in

and out, 15,16,29 which is confirmed by our atomic-resolution STEM characterization (Figure 1d-f). On the basis of these differences, we reasoned that the activation barrier for exchange events should decrease more gradually during anion exchange compared to the sudden change used in previous models for cation exchange in CdSe and ion intercalation in PbBr<sub>2</sub> NCs. 21-23 To test this hypothesis, we used Monte Carlo simulations that yield individual and ensemble nanocrystal transformation trajectories. We obtained the best match with the experimental results with a model in which the energy required for exchanging an anion decreases quadratically with successive events (Figure S19). We refer to this as the exchange-density model because the number of exchanged ions neighboring a site is proportional to the local density of exchanges. The details of these simulations and descriptions of other models tested are provided in the Supporting Information. The quadratic function used in the exchange-density model leads to a more gradual increase in the probability for successive events compared to previous models for NC transformations that lack solid-state miscibility (Figure S20).

The results for the exchange-density model are shown in Figure 4c and Figure S21. The simulated switching times of individual NC trajectories are significantly shorter than the overall switching time corresponding to the ensemble of nanocrystals, in agreement with the experimental data (Figure S21). Furthermore, both the median waiting times and median switching times depend on concentration with the switching times being shorter than the waiting times (Figure 4c). If successive exchange events instead have equal probability, then the waiting and switching times decrease at similar rates with an increase in concentration, and simulated switching times for individual particles occur on the same time scale as the ensemble. On the other hand, models with a steeper drop in activation barrier for exchange events, such as the positivecooperativity model developed by Routzahn and Jain,<sup>2</sup> to a switching time that is independent of concentration (Figure S19). Thus, by assuming the halide concentration is uniform within each nanocrystal during the reaction, in agreement with our STEM results and prior ensemble kinetic studies, 29,30 our exchange-density model correctly describes both the stochasticity of anion exchange at the single-nanocrystal level and the concentration dependence of switching times.

In summary, analyzing the trajectories for single CsPbCl<sub>3</sub> NCs to transform into CsPbBr<sub>3</sub> (and vice versa) reveals a strong dependence for the switching times on the concentration of substitutional halide ions used to induce anion exchange. This concentration dependence has not been observed for other nanocrystal transformations, which we attribute to the lack of miscibility between the initial and final structures in these prior systems. We propose a model in which the energetics for further anion exchange depend on the density of exchanged ions in the nanocrystal; this exchange-density model successfully reproduces all salient features of the reaction observed by single-particle fluorescence. Scaling up the synthesis of CsPbCl<sub>3-x</sub>Br<sub>x</sub> nanocrystals will require homogeneous mixing of both the parent nanocrystals and substitutional halide ions at high concentrations to minimize the effect that the stochastic distribution of waiting times will have on the final halide composition (i.e., value of x) of individual nanocrystals. If reactant-depletion effects are prominent at higher concentrations, nanocrystals with longer waiting times may not undergo the same extent of anion exchange as those with shorter waiting times, leading to greater heterogeneity in composition and lower color purity. One way

to achieve high-throughput synthesis with uniform mixing is through parallel microfluidic reactors as has been demonstrated for the synthesis of cadmium chalcogenide nanocrystals. 56

## ASSOCIATED CONTENT

# **Solution** Supporting Information

The Supporting Information is available free of charge at https://pubs.acs.org/doi/10.1021/acs.jpclett.9b03633.

Materials and Methods, supporting discussion of the method used to identify single nanocrystals in fluorescence videos, effect of flow rate and diffusion, effect of the light intensity and wavelength on the singlenanocrystal trajectories, a comparison of the different Monte Carlo models, figures showing histograms of the edge lengths of the nanocrystals, a comparison of simulated XRD patterns for CsPbBr3 and Cs4PbBr6, Xray photoelectron spectra of the nanocrystal samples, STEM images of nanocrystals on their sides, a comparison of photoluminescence spectra of CsPbBr3 nanocrystals synthesized by hot injection and anion exchange, a schematic of the experimental setup used to monitor anion exchange by fluorescence microscopy, TEM images of CsPbCl<sub>3</sub> nanocrystals deposited at different concentrations, a comparison of intensity trajectories for single nanocrystals prepared in situ and ex situ, intensity trajectories for clusters of particles, waiting times and switching times plotted versus the position of the nanocrystals, plots of the distribution of waiting times at different TBAB concentrations, a comparison of the ensemble intensity rise and the mean switching time at different TBAB concentrations, waiting times and switching times measured using different light intensities and wavelengths, waiting times and switching times for larger CsPbCl<sub>3</sub> nanocrystals, fluorescence trajectories for bromide to chloride anion exchange, a comparison of waiting and switching times for forward and backward exchange, simulated waiting and switching times for different models, changes in free energy and probability for exchange using different models, and simulated reaction trajectories using the exchange-density model, and tables listing the peak maxima and fwhm of ensemble PL spectra, binding energies measured by XPS, fitting parameters for different Monte Carlo models, and the ratios of fitting parameters (PDF)

Movie in which individual nanocrystals become bright as they transform from  $CsPbCl_3$  to  $CsPbCl_{3-x}Br_x$  (MP4) Movie in which individual nanocrystals become dark as they transform from  $CsPbCl_{3-x}Br_x$  to  $CsPbCl_3$  (MP4)

# AUTHOR INFORMATION

#### **Corresponding Author**

Bryce Sadtler — Department of Chemistry and Institute of Materials Science & Engineering, Washington University in St. Louis, St. Louis, Missouri 63130, United States; ⊚ orcid.org/0000-0003-4860-501X; Email: sadtler@wustl.edu

# **Other Authors**

Dong Wang — Department of Chemistry, Washington University in St. Louis, St. Louis, Missouri 63130, United States;
orcid.org/0000-0002-7268-3483

John Cavin — Department of Physics, Washington University in St. Louis, St. Louis, Missouri 63130, United States

- **Bo Yin** Institute of Materials Science & Engineering, Washington University in St. Louis, St. Louis, Missouri 63130, United States
- Arashdeep S. Thind Institute of Materials Science & Engineering, Washington University in St. Louis, St. Louis, Missouri 63130, United States; ⊚ orcid.org/0000-0003-0262-766X
- Albina Y. Borisevich Center for Nanophase Materials Sciences, Oak Ridge National Laboratory, Oak Ridge, Tennnessee 37831, United States; Oorcid.org/0000-0002-3953-8460
- Rohan Mishra Institute of Materials Science & Engineering and Department of Mechanical Engineering and Materials Science, Washington University in St. Louis, St. Louis, Missouri 63130, United States; orcid.org/0000-0003-1261-0087

Complete contact information is available at: https://pubs.acs.org/10.1021/acs.jpclett.9b03633

#### **Notes**

The authors declare no competing financial interest.

### ACKNOWLEDGMENTS

This material is based upon work supported by the National Science Foundation (NSF) under Grant CHE-1753344 to B.S. J.C. was supported through NSF Grant DMREF-CBET-1729787. A.S.T. and R.M. were supported through NSF Grant DMR-1806147. Aberration-corrected STEM experiments were conducted at the Center for Nanophase Materials Sciences at Oak Ridge National Laboratory, which is a Department of Energy (DOE) Office of Science User Facility, through a user project (A.Y.B.). Electron microscopy and X-ray photoelectron spectroscopy were performed at the Institute of Materials Science & Engineering at Washington University at St. Louis. X-ray diffraction was performed in the Department of Earth and Planetary Sciences at Washington University in St. Louis.

# REFERENCES

- (1) Protesescu, L.; Yakunin, S.; Bodnarchuk, M. I.; Krieg, F.; Caputo, R.; Hendon, C. H.; Yang, R. X.; Walsh, A.; Kovalenko, M. V. Nanocrystals of Cesium Lead Halide Perovskites (CsPbX<sub>3</sub>, X = Cl, Br, and I): Novel Optoelectronic Materials Showing Bright Emission with Wide Color Gamut. *Nano Lett.* **2015**, *15*, 3692–3696.
- (2) Butkus, J.; Vashishtha, P.; Chen, K.; Gallaher, J. K.; Prasad, S. K. K.; Metin, D. Z.; Laufersky, G.; Gaston, N.; Halpert, J. E.; Hodgkiss, J. M. The Evolution of Quantum Confinement in CsPbBr<sub>3</sub> Perovskite Nanocrystals. *Chem. Mater.* **2017**, *29*, 3644–3652.
- (3) Cho, J.; Jin, H.; Sellers, D. G.; Watson, D. F.; Son, D. H.; Banerjee, S. Influence of Ligand Shell Ordering on Dimensional Confinement of Cesium Lead Bromide (CsPbBr<sub>3</sub>) Perovskite Nanoplatelets. *J. Mater. Chem. C* 2017, 5, 8810–8818.
- (4) Sapori, D.; Kepenekian, M.; Pedesseau, L.; Katan, C.; Even, J. Quantum Confinement and Dielectric Profiles of Colloidal Nanoplatelets of Halide Inorganic and Hybrid Organic–Inorganic Perovskites. *Nanoscale* **2016**, *8*, 6369–6378.
- (5) Morrell, M. V.; He, X.; Luo, G.; Thind, A. S.; White, T. A.; Hachtel, J. A.; Borisevich, A. Y.; Idrobo, J.-C.; Mishra, R.; Xing, Y. Significantly Enhanced Emission Stability of CsPbBr<sub>3</sub> Nanocrystals Via Chemically Induced Fusion Growth for Optoelectronic Devices. *ACS Applied Nano Materials* **2018**, *1*, 6091–6098.
- (6) Bekenstein, Y.; Koscher, B. A.; Eaton, S. W.; Yang, P.; Alivisatos, A. P. Highly Luminescent Colloidal Nanoplates of Perovskite Cesium Lead Halide and Their Oriented Assemblies. *J. Am. Chem. Soc.* **2015**, 137, 16008–16011.
- (7) Di Stasio, F.; Christodoulou, S.; Huo, N.; Konstantatos, G. Near-Unity Photoluminescence Quantum Yield in CsPbBr<sub>3</sub> Nanocrystal Solid-State Films Via Postsynthesis Treatment with Lead Bromide. *Chem. Mater.* **2017**, *29*, 7663–7667.

- (8) Zhu, F.; Men, L.; Guo, Y.; Zhu, Q.; Bhattacharjee, U.; Goodwin, P. M.; Petrich, J. W.; Smith, E. A.; Vela, J. Shape Evolution and Single Particle Luminescence of Organometal Halide Perovskite Nanocrystals. *ACS Nano* **2015**, *9*, 2948–2959.
- (9) Boote, B. W.; Andaraarachchi, H. P.; Rosales, B. A.; Blome-Fernández, R.; Zhu, F.; Reichert, M. D.; Santra, K.; Li, J.; Petrich, J. W.; Vela, J.; et al. Unveiling the Photo- and Thermal-Stability of Cesium Lead Halide Perovskite Nanocrystals. *ChemPhysChem* **2019**, *20*, 2647—2656
- (10) Zhang, L.; Yang, X.; Jiang, Q.; Wang, P.; Yin, Z.; Zhang, X.; Tan, H.; Yang, Y.; Wei, M.; Sutherland, B. R.; Sargent, E. H.; You, J. Ultra-Bright and Highly Efficient Inorganic Based Perovskite Light-Emitting Diodes. *Nat. Commun.* **2017**, *8*, 15640.
- (11) Van Le, Q.; Jang, H. W.; Kim, S. Y. Recent Advances toward High-Efficiency Halide Perovskite Light-Emitting Diodes: Review and Perspective. *Small Methods* **2018**, *2*, 1700419.
- (12) Wang, K.; Wang, S.; Xiao, S.; Song, Q. Recent Advances in Perovskite Micro- and Nanolasers. *Adv. Opt. Mater.* **2018**, *6*, 1800278.
- (13) Nedelcu, G.; Protesescu, L.; Yakunin, S.; Bodnarchuk, M. I.; Grotevent, M. J.; Kovalenko, M. V. Fast Anion-Exchange in Highly Luminescent Nanocrystals of Cesium Lead Halide Perovskites (CsPbX<sub>3</sub>, X = Cl, Br, I). *Nano Lett.* **2015**, *15*, 5635–5640.
- (14) Jang, D. M.; Park, K.; Kim, D. H.; Park, J.; Shojaei, F.; Kang, H. S.; Ahn, J.-P.; Lee, J. W.; Song, J. K. Reversible Halide Exchange Reaction of Organometal Trihalide Perovskite Colloidal Nanocrystals for Full-Range Band Gap Tuning. *Nano Lett.* **2015**, *15*, 5191–5199.
- (15) Lai, M.; Obliger, A.; Lu, D.; Kley, C. S.; Bischak, C. G.; Kong, Q.; Lei, T.; Dou, L.; Ginsberg, N. S.; Limmer, D. T.; et al. Intrinsic Anion Diffusivity in Lead Halide Perovskites Is Facilitated by a Soft Lattice. *Proc. Natl. Acad. Sci. U. S. A.* **2018**, *115*, 11929–11934.
- (16) Pan, D.; Fu, Y.; Chen, J.; Czech, K. J.; Wright, J. C.; Jin, S. Visualization and Studies of Ion-Diffusion Kinetics in Cesium Lead Bromide Perovskite Nanowires. *Nano Lett.* **2018**, *18*, 1807–1813.
- (17) Son, D. H.; Hughes, S. M.; Yin, Y.; Alivisatos, A. P. Cation Exchange Reactions in Ionic Nanocrystals. *Science* **2004**, *306*, 1009–1012
- (18) Hassan, Y.; Song, Y.; Pensack, R. D.; Abdelrahman, A. I.; Kobayashi, Y.; Winnik, M. A.; Scholes, G. D. Structure-Tuned Lead Halide Perovskite Nanocrystals. *Adv. Mater.* **2016**, *28*, 566–573.
- (19) Chan, E. M.; Marcus, M. A.; Fakra, S.; ElNaggar, M.; Mathies, R. A.; Alivisatos, A. P. Millisecond Kinetics of Nanocrystal Cation Exchange Using Microfluidic X-Ray Absorption Spectroscopy. *J. Phys. Chem. A* **2007**, *111*, 12210–12215.
- (20) Sadtler, B.; Demchenko, D. O.; Zheng, H.; Hughes, S. M.; Merkle, M. G.; Dahmen, U.; Wang, L.-W.; Alivisatos, A. P. Selective Facet Reactivity During Cation Exchange in Cadmium Sulfide Nanorods. *J. Am. Chem. Soc.* **2009**, *131*, 5285–5293.
- (21) Routzahn, A. L.; Jain, P. K. Luminescence Blinking of a Reacting Quantum Dot. *Nano Lett.* **2015**, *15*, 2504–2509.
- (22) Routzahn, A. L.; Jain, P. K. Single-Nanocrystal Reaction Trajectories Reveal Sharp Cooperative Transitions. *Nano Lett.* **2014**, 14, 987–992.
- (23) Yin, B.; Cavin, J.; Wang, D.; Khan, D.; Shen, M.; Laing, C.; Mishra, R.; Sadtler, B. Fluorescence Microscopy of Single Lead Bromide Nanocrystals Reveals Sharp Transitions During Their Transformation to Methylammonium Lead Bromide. *J. Mater. Chem. C* **2019**, *7*, 3486–3495.
- (24) Liu, Z.; Bekenstein, Y.; Ye, X.; Nguyen, S. C.; Swabeck, J.; Zhang, D.; Lee, S.-T.; Yang, P.; Ma, W.; Alivisatos, A. P. Ligand Mediated Transformation of Cesium Lead Bromide Perovskite Nanocrystals to Lead Depleted Cs<sub>4</sub>PbBr<sub>6</sub> Nanocrystals. *J. Am. Chem. Soc.* **2017**, *139*, 5309–5312.
- (25) Wu, L.; Hu, H.; Xu, Y.; Jiang, S.; Chen, M.; Zhong, Q.; Yang, D.; Liu, Q.; Zhao, Y.; Sun, B.; et al. From Nonluminescent  $Cs_4PbX_6$  (X = Cl, Br, I) Nanocrystals to Highly Luminescent  $CsPbX_3$  Nanocrystals: Water-Triggered Transformation through a CsX-Stripping Mechanism. *Nano Lett.* **2017**, *17*, 5799–5804.
- (26) Akkerman, Q. A.; Park, S.; Radicchi, E.; Nunzi, F.; Mosconi, E.; De Angelis, F.; Brescia, R.; Rastogi, P.; Prato, M.; Manna, L. Nearly

- Monodisperse Insulator  $Cs_4PbX_6$  (X = Cl, Br, I) Nanocrystals, Their Mixed Halide Compositions, and Their Transformation into  $CsPbX_3$  Nanocrystals. *Nano Lett.* **2017**, *17*, 1924–1930.
- (27) Li, M.; Zhang, X.; Dong, T.; Wang, P.; Matras-Postolek, K.; Yang, P. Evolution of Morphology, Phase Composition, and Photoluminescence of Cesium Lead Bromine Nanocrystals with Temperature and Precursors. *J. Phys. Chem. C* 2018, 122, 28968–28976.
- (28) Li, M.; Zhang, X.; Matras-Postolek, K.; Chen, H.-S.; Yang, P. An Anion-Driven Sn<sup>2+</sup> Exchange Reaction in CsPbBr<sub>3</sub> Nanocrystals Towards Tunable and High Photoluminescence. *J. Mater. Chem. C* **2018**, *6*, 5506–5513.
- (29) Koscher, B. A.; Bronstein, N. D.; Olshansky, J. H.; Bekenstein, Y.; Alivisatos, A. P. Surface- Vs Diffusion-Limited Mechanisms of Anion Exchange in CsPbBr<sub>3</sub> Nanocrystal Cubes Revealed through Kinetic Studies. *J. Am. Chem. Soc.* **2016**, *138*, 12065–12068.
- (30) Loiudice, A.; Strach, M.; Saris, S.; Chernyshov, D.; Buonsanti, R. Universal Oxide Shell Growth Enables in Situ Structural Studies of Perovskite Nanocrystals During the Anion Exchange Reaction. *J. Am. Chem. Soc.* **2019**, *141*, 8254–8263.
- (31) Yin, W.-J.; Yan, Y.; Wei, S.-H. Anomalous Alloy Properties in Mixed Halide Perovskites. J. Phys. Chem. Lett. 2014, 5, 3625–3631.
- (32) Bechtel, J. S.; Van der Ven, A. First-Principles Thermodynamics Study of Phase Stability in Inorganic Halide Perovskite Solid Solutions. *Phys. Rev. Mater.* **2018**, *2*, 045401.
- (33) Empedocles, S.; Bawendi, M. Spectroscopy of Single CdSe Nanocrystallites. *Acc. Chem. Res.* **1999**, *32*, 389–396.
- (34) Orfield, N. J.; McBride, J. R.; Keene, J. D.; Davis, L. M.; Rosenthal, S. J. Correlation of Atomic Structure and Photoluminescence of the Same Quantum Dot: Pinpointing Surface and Internal Defects That Inhibit Photoluminescence. *ACS Nano* **2015**, *9*, 831–839.
- (35) Park, Y.-S.; Guo, S.; Makarov, N. S.; Klimov, V. I. Room Temperature Single-Photon Emission from Individual Perovskite Quantum Dots. ACS Nano 2015, 9, 10386–10393.
- (36) Rainò, G.; Nedelcu, G.; Protesescu, L.; Bodnarchuk, M. I.; Kovalenko, M. V.; Mahrt, R. F.; Stöferle, T. Single Cesium Lead Halide Perovskite Nanocrystals at Low Temperature: Fast Single-Photon Emission, Reduced Blinking, and Exciton Fine Structure. *ACS Nano* **2016**, *10*, 2485–2490.
- (37) Utzat, H.; Shulenberger, K. E.; Achorn, O. B.; Nasilowski, M.; Sinclair, T. S.; Bawendi, M. G. Probing Linewidths and Biexciton Quantum Yields of Single Cesium Lead Halide Nanocrystals in Solution. *Nano Lett.* **2017**, *17*, 6838–6846.
- (38) Yarita, N.; Tahara, H.; Saruyama, M.; Kawawaki, T.; Sato, R.; Teranishi, T.; Kanemitsu, Y. Impact of Postsynthetic Surface Modification on Photoluminescence Intermittency in Formamidinium Lead Bromide Perovskite Nanocrystals. *J. Phys. Chem. Lett.* **2017**, *8*, 6041–6047.
- (39) Freppon, D. J.; Men, L.; Burkhow, S. J.; Petrich, J. W.; Vela, J.; Smith, E. A. Photophysical Properties of Wavelength-Tunable Methylammonium Lead Halide Perovskite Nanocrystals. *J. Mater. Chem. C* 2017, *5*, 118–126.
- (40) Zhang, A.; Dong, C.; Ren, J. Tuning Blinking Behavior of Highly Luminescent Cesium Lead Halide Nanocrystals through Varying Halide Composition. *J. Phys. Chem. C* **2017**, *121*, 13314–13323.
- (41) Gibson, N. A.; Koscher, B. A.; Alivisatos, A. P.; Leone, S. R. Excitation Intensity Dependence of Photoluminescence Blinking in CsPbBr<sub>3</sub> Perovskite Nanocrystals. *J. Phys. Chem. C* **2018**, *122*, 12106–12113.
- (42) Seth, S.; Ahmed, T.; Samanta, A. Photoluminescence Flickering and Blinking of Single CsPbBr<sub>3</sub> Perovskite Nanocrystals: Revealing Explicit Carrier Recombination Dynamics. *J. Phys. Chem. Lett.* **2018**, *9*, 7007–7014.
- (43) Yuan, G.; Ritchie, C.; Ritter, M.; Murphy, S.; Gómez, D. E.; Mulvaney, P. The Degradation and Blinking of Single CsPbI<sub>3</sub> Perovskite Quantum Dots. *J. Phys. Chem. C* **2018**, *122*, 13407–13415.
- (44) Tian, Y.; Merdasa, A.; Peter, M.; Abdellah, M.; Zheng, K.; Ponseca, C. S.; Pullerits, T.; Yartsev, A.; Sundström, V.; Scheblykin, I. G. Giant Photoluminescence Blinking of Perovskite Nanocrystals

- Reveals Single-Trap Control of Luminescence. *Nano Lett.* **2015**, *15*, 1603–1608.
- (45) Ryan, D. P.; Goodwin, P. M.; Sheehan, C. J.; Whitcomb, K. J.; Gelfand, M. P.; Van Orden, A. Mapping Emission from Clusters of CdSe/ZnS Nanoparticles. *J. Phys. Chem. C* **2018**, *122*, 4046–4053.
- (46) Pennycook, S. J.; Jesson, D. E. High-Resolution Z-Contrast Imaging of Crystals. *Ultramicroscopy* **1991**, *37*, 14–38.
- (47) Linaburg, M. R.; McClure, E. T.; Majher, J. D.; Woodward, P. M.  $Cs_{1-x}Rb_xPbCl_3$  and  $Cs_{1-x}Rb_xPbCl_3$  Solid Solutions: Understanding Octahedral Tilting in Lead Halide Perovskites. *Chem. Mater.* **2017**, *29*, 3507–3514.
- (48) Akkerman, Q. A.; Motti, S. G.; Srimath Kandada, A. R.; Mosconi, E.; D'Innocenzo, V.; Bertoni, G.; Marras, S.; Kamino, B. A.; Miranda, L.; De Angelis, F.; et al. Solution Synthesis Approach to Colloidal Cesium Lead Halide Perovskite Nanoplatelets with Monolayer-Level Thickness Control. *J. Am. Chem. Soc.* **2016**, *138*, 1010–1016.
- (49) Abdelmageed, G.; Jewell, L.; Hellier, K.; Seymour, L.; Luo, B.; Bridges, F.; Zhang, J. Z.; Carter, S. Mechanisms for Light Induced Degradation in MAPbI<sub>3</sub> Perovskite Thin Films and Solar Cells. *Appl. Phys. Lett.* **2016**, *109*, 233905.
- (50) Draguta, S.; Sharia, O.; Yoon, S. J.; Brennan, M. C.; Morozov, Y. V.; Manser, J. S.; Kamat, P. V.; Schneider, W. F.; Kuno, M. Rationalizing the Light-Induced Phase Separation of Mixed Halide Organic—Inorganic Perovskites. *Nat. Commun.* **2017**, *8*, 200.
- (51) Song, Z.; Wang, C.; Phillips, A. B.; Grice, C. R.; Zhao, D.; Yu, Y.; Chen, C.; Li, C.; Yin, X.; Ellingson, R. J.; et al. Probing the Origins of Photodegradation in Organic—Inorganic Metal Halide Perovskites with Time-Resolved Mass Spectrometry. *Sustainable Energy & Fuels* **2018**, *2*, 2460–2467.
- (52) Liu, L.; Deng, L.; Huang, S.; Zhang, P.; Linnros, J.; Zhong, H.; Sychugov, I. Photodegradation of Organometal Hybrid Perovskite Nanocrystals: Clarifying the Role of Oxygen by Single-Dot Photoluminescence. *J. Phys. Chem. Lett.* **2019**, *10*, 864–869.
- (53) Yang, J.-H.; Yin, W.-J.; Park, J.-S.; Wei, S.-H. Fast Self-Diffusion of Ions in CH<sub>3</sub>NH<sub>3</sub>PbI<sub>3</sub>: The Interstiticaly Mechanism Versus Vacancy-Assisted Mechanism. *J. Mater. Chem. A* **2016**, *4*, 13105–13112.
- (54) Ott, F. D.; Spiegel, L. L.; Norris, D. J.; Erwin, S. C. Microscopic Theory of Cation Exchange in CdSe Nanocrystals. *Phys. Rev. Lett.* **2014**, *113*, 156803.
- (55) Senocrate, A.; Moudrakovski, I.; Kim, G. Y.; Yang, T.-Y.; Gregori, G.; Grätzel, M.; Maier, J. The Nature of Ion Conduction in Methylammonium Lead Iodide: A Multimethod Approach. *Angew. Chem., Int. Ed.* **2017**, *56*, 7755–7759.
- (56) Nightingale, A. M.; Bannock, J. H.; Krishnadasan, S. H.; O'Mahony, F. T. F.; Haque, S. A.; Sloan, J.; Drury, C.; McIntyre, R.; deMello, J. C. Large-Scale Synthesis of Nanocrystals in a Multichannel Droplet Reactor. *J. Mater. Chem. A* **2013**, *1*, 4067–4076.